



1 Chlorine enhances nocturnal heterogeneous uptake of NO₂ in 2 coastal atmosphere under sea-land breeze circulation

3 Ziyi Lin^{1,2,3}, Xiuwen Yong^{1,2,4}, Lingjun Li^{1,2,3}, Yuping Chen^{1,2,3}, Lingling Xu^{1,2,3*},
4 Xiaoting Ji^{1,2,3}, Chen Yang^{1,2,3}, Keran Zhang^{1,2,3}, Feng Zhang,^{1,2} Ziyang Chen^{1,2,3}, Gaojie
5 Chen^{1,2,3}, Xiaolong Fan^{1,2}, Mengren Li^{1,2}, Jinsheng Chen^{1,2,3*}

6 7 Affiliations:

8 ¹State Key Laboratory of Advanced Environmental Technology, Institute of Urban Environment, Chinese
9 Academy of Sciences, Xiamen 361021, China

10 ²Fujian Key Laboratory of Atmospheric Ozone Pollution Prevention, Institute of Urban Environment,
11 Chinese Academy of Sciences, Xiamen 361021, China

12 ³University of Chinese Academy of Sciences, Beijing 100049, China

13 ⁴Fujian Agriculture and Forestry University, Fuzhou, 350002, China

14
15 *Correspondence to: jschen@iue.ac.cn (Jinsheng Chen); Linglingxu@iue.ac.cn (Lingling Xu)

16
17 **Abstract:** Heterogeneous uptake of NO₂ serves as a significant source for reactive nitrogen species,
18 playing an important role in atmospheric chemistry. Laboratory studies have demonstrated that
19 chlorine can promote the heterogeneous NO₂ uptake, yet this effect under real ambient conditions
20 remains poorly elucidated. Based on comprehensive field observations, a machine learning
21 technique, and a multiphase chemical box model in the coastal city of Xiamen, China, this study
22 reveals the enhancement effect of chlorine (Cl) on NO₂ uptake and quantifies the impact of this
23 enhanced uptake on reactive nitrogen species during nocturnal sea-land breeze (SLB) periods.
24 Compared with non-SLB days, nocturnal concentrations of nitrous acid (HONO) and particulate
25 nitrate (NO₃⁻) increased significantly during SLB days, with high mean value of NO₂ uptake rate
26 constant (kNO₂) reaching 9.70×10⁻⁶ s⁻¹. Machine learning revealed that chlorine was the most
27 important influencing factor for the enhanced kNO₂. Incorporating this kNO₂ into the chemical box
28 model substantially resolved the underestimation of HONO concentration and NO₃⁻ production
29 under SLB conditions. Notably, nocturnal NO₂ uptake dominated HONO formation (83.9%), while
30 making a substantial contribution (47.9%) to nitrate formation. This study highlights the critical role
31 of chlorine-enhanced NO₂ uptake in atmospheric reactive nitrogen cycling and provides valuable
32 insights for nocturnal chemistry in complex coastal environments.

33 34 1. Introduction

35 Nitrous acid (HONO) and nitrate (NO₃⁻) are key reactive nitrogen species in the atmosphere. HONO,
36 a major source of OH radicals, significantly contributes to the formation of O₃ and secondary
37 aerosols by influencing radical budget (Acker et al., 2006; Alicke et al., 2003). NO₃⁻ is an important
38 chemical component of particulate matter (PM), contributing to PM pollution and acid rain (Cao et
39 al., 2022; Qu and Han, 2021). As a crucial source of both HONO and NO₃⁻, the heterogeneous
40 uptake of NO₂ has attracted considerable attention (Xuan et al., 2025; Carter et al., 1982).

41 Traditionally, the uptake of NO₂ in bulk solution was considered extremely slow, and thus this
42 process was often negligible (Lee and Schwartz, 1981). However, numerous field observations have
43 indicated that NO₂ uptake plays a significant role in the formation of HONO and NO₃⁻. Previous
44 studies have revealed a strong correlation between NO₂ and HONO after excluding homogeneous
45 formation and primary emissions, suggesting efficient heterogeneous conversion of NO₂ to HONO



46 (Su et al., 2008; Zhang et al., 2024). Studies have also found that incorporating NO₂ uptake
47 mechanisms into models can substantially improve the HONO simulation, especially at night
48 (Zhang et al., 2023; Xuan et al., 2024; Zhang et al., 2024; Shi et al., 2020). Using an aerosol-fog
49 sampling system and a box model, Xu et al (Xu et al., 2024), found that NO₂ uptake was the primary
50 driver of the rapid increase in NO₃⁻ during fog events. Currently, the reported reaction rate constant
51 for NO₂ uptake vary widely across different types of surfaces, spanning several orders of magnitude
52 from 10⁻⁷ s⁻¹ to 10⁻⁵ s⁻¹ (Zhang et al., 2025b). Multiple factors have been demonstrated to affect the
53 NO₂ uptake rate constant (kNO₂) in laboratories, including NO₂ concentrations, aerosol particle size,
54 ionic strength, pH, NH₃, and liquid water content (Liu and Abbatt, 2021; Gen et al., 2024; Zhang et
55 al., 2025a). In the real atmosphere, research during haze events showed that parameterization
56 schemes of kNO₂ considering relative humidity (RH) and NH₃ influences significantly improved
57 the simulation results of heterogeneous HONO formation (Zhang et al., 2023). Long-term
58 observations revealed that changes in aerosol chemical composition could alter aerosol pH,
59 consequently affecting the uptake kinetics of NO₂ to HONO (Zhang et al., 2025b).

60 Investigations in coastal areas reported higher NO₂ uptake rates in marine air masses compared
61 to continental ones (Zha et al., 2014; Yang et al., 2021), overall surpassing those measured at
62 continental urban, suburban, and rural sites (Wentzell et al., 2010; Kleffmann et al., 2003; Zhang et
63 al., 2020; Hao et al., 2020; Cui et al., 2018). These findings suggests that heterogeneous NO₂ uptake
64 plays a particularly critical role in the coastal troposphere. Within the marine boundary layer,
65 chloride ions are abundant due to sea spray. Chloride ions exhibit special surface propensity, making
66 them tend to distribute at the air-water interface (Knipping et al., 2000; Piatkowski et al., 2014;
67 Jungwirth and Tobias, 2006). Laboratory studies demonstrated that chloride ions can establish a
68 surface-directed electric field, which attracts atmospheric NO₂ molecules and promotes their further
69 uptake at air-water interface (Wang et al., 2025a; Zhang et al., 2025a). Nevertheless, the influence
70 of chlorine on NO₂ uptake in realistic coastal atmosphere and the consequent impacts on reactive
71 nitrogen cycling remain to be fully elucidated.

72 Sea-land breeze (SLB) events occur frequently in coastal urban areas (Chen et al., 2023; Liu et
73 al., 2025; Xie et al., 2023). During SLB periods, the coastal boundary layer experiences intensive
74 interactions between marine and continental air masses, providing a natural laboratory to investigate
75 the effect of sea-salt chloride on NO₂ uptake. In this study, a multi-parameter field observation was
76 conducted in Xiamen, a typical coastal city in China, during the autumn and winter seasons
77 characterized by frequent SLB events (Chen et al., 2023). Based on observations, the characteristics
78 of SLB days were revealed and kNO₂ under both SLB and non-SLB conditions were quantified.
79 Using machine learning method, the significant promoting effect of chlorine on NO₂ uptake during
80 nocturnal SLB periods was demonstrated. Furthermore, the obtained kNO₂ was incorporated into
81 an advanced multiphase box model to evaluate the impact of chlorine-enhanced NO₂ uptake on
82 atmospheric reactive nitrogen cycling. This study highlights the role of previously overlooked
83 chlorine on NO₂ uptake for nocturnal chemistry in coastal atmosphere.

84

85 **2. Methods**

86 **2.1 Field measurements and sea-land breeze identification**

87 Our observations were conducted at the Atmospheric Observation Supersite (24.61°N, 118.06°E)
88 of the Institute of Urban Environment (IUE), Chinese Academy of Sciences in Xiamen, from
89 November 18, 2023 to January 6, 2024. Xiamen is a coastal city in southeastern China. The



90 observation site is located approximately 5 km from the shore and is surrounded by residential,
 91 commercial areas and major traffic arteries. Instruments were deployed on the roof of the IUE
 92 building at approximately 70 m above ground level. Virtually no high buildings obstructed the path
 93 between the site and the coast, making it a typical coastal urban site.

94 A suite of atmospheric parameters was observed simultaneously. Ambient HONO was
 95 measured online by a water-based long-path absorption photometer (Zhichen Beijing, China) (Xuan
 96 et al., 2024). Sulfuric acid (H_2SO_4) and HCl were measured using a long time-of-flight chemical
 97 ionization mass spectrometer, equipped with a nitrate reagent ion source (Aerodyne Research Inc.,
 98 USA) (Yang et al., 2023). The chemical composition of $PM_{2.5}$ was analyzed using both a MARGA
 99 ADI 2080 (Metrohm Applikon, Switzerland) and an ACSM (Aerodyne Research Inc., USA) (Liu
 100 et al., 2022; Chen et al., 2022). Particle number size distribution (PNSD) in the range of 2–300 nm
 101 was measured by two scanning mobility particle sizers (TSI inc., USA) equipped with a long-DMA
 102 (2.5–62 nm) and a nano-DMA (7–300 nm), respectively (Li et al., 2025). Additionally, a range of
 103 commercial instruments were employed to monitor trace gases (NO, NO_2 , SO_2 , O_3 , and VOCs),
 104 meteorological parameters (ambient temperature, RH, wind-speed, wind-direction and ultraviolet
 105 radiation), and photolysis rates (J^{O^1D} , J^{NO_2} , J^{HONO} , J^{NO_3} , J^{HCHO} and $J^{H_2O_2}$) (Liu et al., 2022).
 106 Detailed descriptions of instrument operation, species identification, and calibration are provided in
 107 **Text S1**. Hourly BLH data were obtained from the ERA5 reanalysis dataset (Hersbach et al., 2020).

108 Sea-land breeze days were identified based on observed wind-speed and wind-direction
 109 according to the criteria established in our previous work (Chen et al., 2023). Briefly, the coastline
 110 in Xiamen is characterized by a northeast-southwest trend, the sea breeze is blowing from the east-
 111 south, and the land breeze is blowing from the west-north-northeast. According to observed wind
 112 direction, a natural day could be divided into four periods. Specifically, 01:00-08:00 LT (land breeze
 113 period), 13:00-20:00 LT (sea breeze period), and 09:00-12:00 LT and 21:00-24:00 LT (mixed sea-
 114 land breeze period). A day was classified as an SLB day if the following three conditions were met:
 115 (1) the 24-hour mean wind speed was < 10 m/s; (2) during the land breeze period, the land breeze
 116 persisted for ≥ 4 hours and the sea breeze lasted ≤ 2 hours; and (3) during the sea breeze period, sea
 117 breeze persisted for ≥ 4 hours and the land breeze lasted ≤ 2 hours. As shown in **Fig. S1** (light blue
 118 areas), a total of 23 SLB days were identified during the observation period. The remaining days
 119 were classified as non-SLB days. **Fig. S2** illustrates that the wind patterns on SLB days differed
 120 from those on non-SLB days, characterized by a higher prevalence of southeasterly sea breezes.

121

122 2.2 Calculation of HONO from heterogeneous formation processes and NO_2 uptake rate

123 Due to the absence of agricultural fields near the sampling site and its proximity to major traffic
 124 arteries, the primary emission of HONO was attributed to vehicles. Only nighttime data were used
 125 in our study, the uncertainties associated with photochemical process, such as NO_3 photolysis were
 126 excluded. Therefore, the nighttime corrected HONO ($HONO_{corr}$) is calculated as follows:

$$127 \quad HONO_{corr,t} = HONO_t - E_{vehicle,t} - P_{NO+OH,t} \quad (1)$$

128 where $HONO_t$ is the observed HONO concentration, $E_{vehicle,t}$ is the HONO emission from vehicles,
 129 and $P_{NO+OH,t}$ is the HONO production from homogeneous reactions. $E_{vehicle,t}$ is calculated as the NO_x
 130 concentration multiplied by the emission factor 0.005, which was set as a lower limit to prevent
 131 underestimating the secondary formation of HONO (Zhang et al., 2025b). $P_{NO+OH,t}$ is calculated as
 132 follows:

$$133 \quad P_{NO+OH,t} = k_{NO+OH} \times [NO] \times [OH] \quad (2)$$



134 where $k_{\text{NO}+\text{OH}}$ ($\text{cm}^3/\text{molecules/s}$) is calculated in the Master Chemical Mechanism 3.3.1 (MCM
135 v3.3.1 <https://mcm.york.ac.uk/MCM/>), and the concentration of OH radicals is estimated based on
136 the steady-state balance of H_2SO_4 (Nie et al., 2022). Because H_2SO_4 is primarily produced by the
137 reaction of SO_2 and OH and is mainly lost via condensation sink (CS) onto particle surfaces, the OH
138 concentration can be estimated as below:

$$139 \quad [\text{OH}] = \frac{[\text{H}_2\text{SO}_4] \times \text{CS}}{k_{\text{OH}+\text{SO}_2} \times [\text{SO}_2]} \quad (3)$$

140 where $k_{\text{OH}+\text{SO}_2}$ is $5 \times 10^{-13} \text{ cm}^3/\text{s}$ (Seinfeld et al., 1998), and CS (/s) is calculated as follows (Kulmala
141 et al., 2012):

$$142 \quad \text{CS} = 2\pi D_v \int_0^{d_{p,\text{max}}} d_p \beta n(d_p) dd_p \quad (4)$$

143 where D_v is the diffusion coefficient of H_2SO_4 , d_p is the particle diameter derived from the measured
144 PNSD, β is the transitional correction factor, and $n(d_p)$ is the particle number concentration of
145 diameter d_p .

146 In line with previous studies (Zhang et al., 2025b; Zhang et al., 2020; Zhang et al., 2024), the
147 variation in the $\text{HONO}_{\text{corr}}/\text{NO}_2$ ratio (equation 5) was applied to calculate the reaction rate constant
148 of NO_2 uptake (k_{NO_2}) in our study as follows:

$$149 \quad k_{\text{NO}_2} = \frac{\text{HONO}_{\text{corr},t_2} - \text{HONO}_{\text{corr},t_1}}{\overline{\text{NO}_2}(t_2 - t_1)} \quad (5)$$

150 where $\overline{\text{NO}_2}$ is the mean concentration of NO_2 between t_1 and t_2 .

151

152 2.3 Machine learning technique

153 Random Forest (RF) algorithm, a machine learning technique extensively applied in atmospheric
154 (Yang et al., 2024; Lin et al., 2026a; Zhang et al., 2025b), was employed to elucidate the primary
155 drivers of k_{NO_2} . The model was built using the “scikit-learn” library ([https://github.com/scikit-
156 learn/scikit-learn/blob/fe2edb3cd/sklearn/ensemble/](https://github.com/scikit-learn/scikit-learn/blob/fe2edb3cd/sklearn/ensemble/), last access: June 10, 2026) in a python
157 environment. Drawing upon previously identified factors influencing k_{NO_2} (e.g., pH, RH, NH_3)
158 (Liu and Abbatt, 2021; Gen et al., 2024; Zhang et al., 2025a; Zhang et al., 2023) alongside the
159 specific characteristics of the coastal urban environment, we incorporated meteorological
160 parameters (RH and T), atmospheric reactive species (Cl_{total} , NH_3 , and NO_2), and heterogeneous-
161 related parameters (pH, SA, and ground surfaces areas) as input variables for the RF model. To
162 account for the chloride depletion phenomenon, Cl_{total} was utilized as a proxy to represent overall
163 chlorine levels. Only nighttime data was trained in model to eliminate the effects of photochemical
164 processes on k_{NO_2} quantification, thereby enabling a more precise identification of key drivers.
165 Detailed RF hyperparameter configurations and model evaluation are provided in **Text S2**. In this
166 study, the dominant factors were identified based on RF factor importance, which quantifies the
167 percentage contribution of each variable to k_{NO_2} (Breiman, 2001; Gregorutti et al., 2017).
168 Furthermore, one-dimensional partial dependence plots (PDPs) were employed to delineate the main
169 effects of individual variables, while bivariate PDPs were utilized to visualize and accesses the
170 interaction effects between pairs of factors on k_{NO_2} (Goldstein et al., 2015).

171

172 **Multiphase chemical box model.** The multiphase chemical box model was established based on
173 the Framework for 0-D Atmospheric Modeling (F0AM) (Wolfe et al., 2016). As shown in **Table**
174 **S1** and **Table S2**, comprehensive HONO and NO_3^- budgets were incorporated into the F0AM model



175 to simulate the variations of HONO and NO_3^- . The ISORROPIA II model (Seinfeld et al., 1998)
176 was integrated into the model to determine aerosol pH, aerosol liquid water content and the
177 partitioning ratio of HNO_3 and NO_3^- . This study designed six simulation scenarios: excluding the
178 NO_2 uptake mechanism in simulation on (1) SLB and (2) non-SLB days; including NO_2 uptake with
179 the calculated mean kNO_2 on (3) SLB and (4) non-SLB days; and including NO_2 uptake on SLB
180 days using the (5) 25th and (6) 75th percentiles of the calculated kNO_2 . The ability of the model to
181 reproduce real atmospheric processes was evaluated by comparing the simulated HONO and NO_3^-
182 with observations. Due to the underestimation of total particulate nitrate concentrations measured
183 by instruments, the performance of NO_3^- simulations was evaluated by comparing the trends of the
184 simulated NO_3^- production rate with the observed NO_3^- concentration. In contrast, as HONO
185 predominantly exists in the gas phase, the simulated HONO was evaluated directly against the
186 observed HONO concentrations.

187 As for the model simulation, each simulation was preceded by a 3-day spin-up to allow
188 intermediate species concentrations to stabilize. The mean diurnal pattern of trace gas
189 concentrations, meteorological parameters, and the results from the ISORROPIA II model during
190 SLB days and non-SLB days were used as input data to constrain the box model. Notably, the
191 concentrations of HONO and NO_3^- were not constrained by observed values. More details about the
192 model incorporating mechanisms, modules, and simulation settings are provided in **Text S3** and our
193 previous study (Lin et al., 2026b).

194

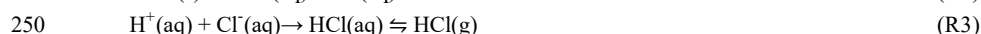
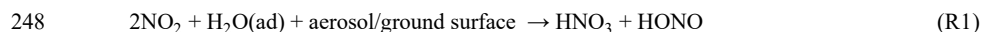
195 **3 Results and discussion**

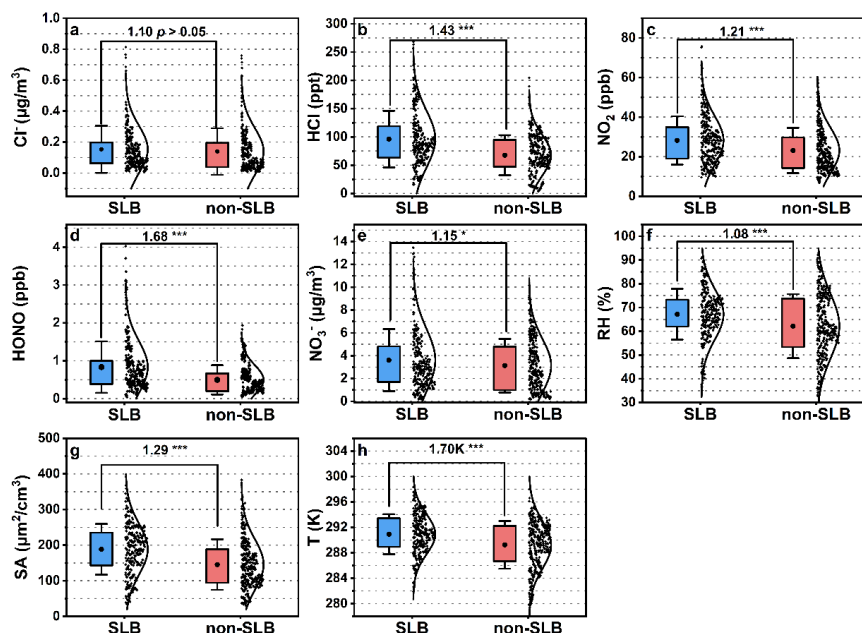
196 **3.1 Characteristics of atmospheric species during SLB days**

197 **Fig. S1** shows the time series of the observed parameters. Based on the identification criteria detailed
198 in the Methods section, 23 days were classified as SLB days, accounting for 48% of entire
199 observation period. The diurnal patterns of major observed parameters are summarized in **Fig. S3**,
200 revealing that the primary differences between the two types of days predominantly emerged at
201 night. Compared to non-SLB days, SLB days exhibited rapid nighttime accumulation of HONO and
202 NO_3^- , accompanied by elevated chlorine levels, NO_x concentrations, and aerosol surface area (SA)
203 concentrations. Additionally, consistent with our previous study, SLB days were characterized by
204 higher temperature and RH at night (Chen et al., 2022). **Fig. 1** and **Table S3** further summarizes the
205 nighttime observational results on SLB and non-SLB days. By definition, SLB days are influenced
206 by persistent sea breezes, which likely enhances the impact of sea-salt aerosols. As shown in **Fig.**
207 **1a**, the particulate chloride (Cl^-) concentrations were comparatively higher on SLB days (0.154
208 $\mu\text{g}/\text{m}^3$) than on non-SLB days ($0.139 \mu\text{g}/\text{m}^3$). Specifically, this overall increase (**Fig. S4**) was
209 primarily driven by elevated levels during the sea breeze (18:00-20:00 LT) and mixed sea-land
210 breeze (21:00-00:00 LT) periods, while concentrations declined during the land breeze (01:00-06:00
211 LT) period. The elevation pattern of Cl^- indicates that the more abundant Cl^- transported by stronger
212 sea breezes on SLB days can persist into the subsequent mixed sea-land breeze periods. Additionally,
213 **Fig. S5** shows that the Na^+-Cl^- correlation was strong on SLB days ($r = 0.67$), while it was weak on
214 non-SLB days ($r = 0.28$). Since sodium chloride (NaCl) is a major component of sea-salt, the
215 stronger Na^+-Cl^- correlation on SLB days than on non-SLB days indicates that sea salt is indeed an
216 important source of Cl^- on SLB days. As for gaseous chlorine, **Fig. 1b** shows that the concentration
217 of gaseous hydrogen chloride (HCl) was significantly higher on SLB days (96.2 ppt) than on non-
218 SLB days (67.5 ppt). This further confirms that, under the influence of sea-salt aerosols on SLB



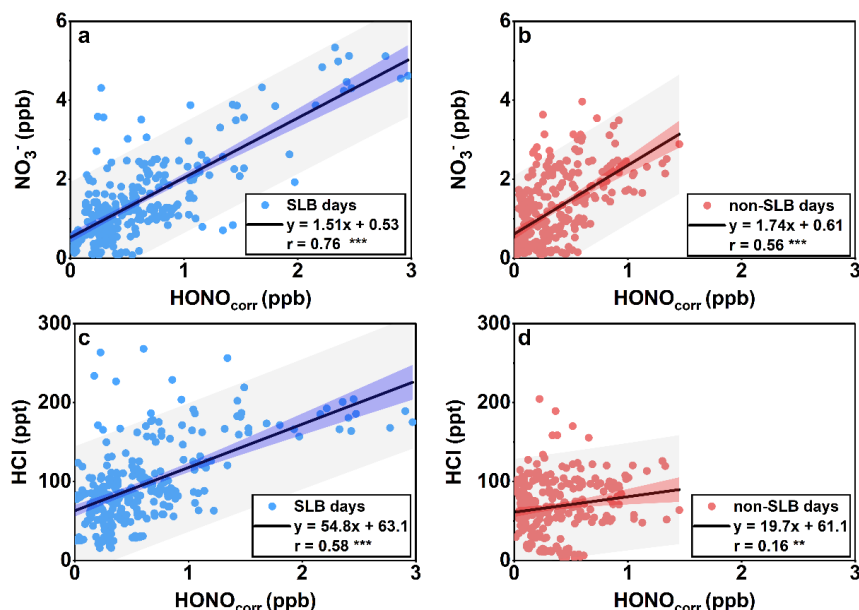
219 days, chlorine levels are distinctly elevated in the nighttime coastal troposphere.
220 **Fig. 1c** indicates that the concentration of NO_2 on SLB days (mean: 28.3 ppb) was significantly
221 higher than that on non-SLB days (23.2 ppb). Within our study area, ship emissions, cross-sea bridge
222 traffic, and road traffic contribute substantial NO_x , and the enhanced local circulation on SLB days
223 can promote NO_2 accumulation (Chen et al., 2023). The mean concentrations of HONO and NO_3^-
224 on SLB day were 0.836 ppb and $3.61 \mu\text{g}/\text{m}^3$, respectively, which were significantly higher than the
225 corresponding values of 0.497 ppb and $3.13 \mu\text{g}/\text{m}^3$ on non-SLB days (**Figs. 1d-1e**). To better
226 understand the elevated HONO levels, $\text{HONO}_{\text{corr}}$ concentrations, defining as the observed HONO
227 concentration subtracts contributions from primary emissions and gas-phase production, were
228 calculated to represent the nocturnal HONO produced from heterogeneous conversion. The ratio of
229 $\text{HONO}_{\text{corr}}/\text{NO}_2$ was notably higher on SLB days (0.030) than on non-SLB days (0.021), indicating
230 more active heterogeneous conversion of NO_2 to HONO on SLB days. Multiple studies have
231 confirmed that NO_2 uptake is a primary source of nocturnal heterogeneous HONO formation (Zhang
232 et al., 2023; Zhang et al., 2022). Here, the higher SA concentrations on SLB days were also
233 conducive to heterogeneous reactions (**Fig. 1g**). Furthermore, **Figs. 2a-2b** indicate a strong
234 correlation between $\text{HONO}_{\text{corr}}$ and NO_3^- , with the correlation coefficient (r) increasing from 0.56 on
235 non-SLB days to 0.76 on SLB days. As shown in reaction 1, NO_2 uptake via disproportionation
236 simultaneously produces HONO and HNO_3 , the latter of which is further converted to NO_3^- via gas-
237 particle partitioning. Thus, nocturnal NO_2 uptake is also likely an important contributor to the
238 formations of NO_3^- on SLB days. **Fig 2c-2d** show that the correlation of $\text{HONO}_{\text{corr}}$ with gaseous
239 HCl was significantly elevated on SLB days ($r = 0.58$) than on non-SLB days ($r = 0.16$), reflecting
240 a strong coupling between NO_2 uptake and chlorine activation under high halogen conditions. The
241 H^+ generated by NO_2 uptake can combine with Cl^- (reactions 2-3). Simultaneously, the aerosol pH
242 in the coastal region of southeastern China was relatively low (approximately 1.92 ± 0.34 during
243 nocturnal SLB periods), chloride depletion could easily occur, leading to the observed positive
244 correlation between $\text{HONO}_{\text{corr}}$ and HCl. The enhanced chloride depletion can also explain our
245 observations of a significant increase in gaseous HCl but not in Cl^- concentrations on SLB days.
246 Similarly, the rapid decline in Cl^- concentration during land breeze periods (**Fig. S4**) could also be
247 explained by chloride depletion.





251

252 Figure 1. Box plots of key observed parameters during nocturnal SLB and non-SLB periods. (a) Cl⁻,
 253 (b) HCl, (c) NO₂, (d) HONO, (e) NO₃⁻, (f) RH, (g) SA, and (h) ambient temperature (T). The box
 254 box shows the 25th–75th percentiles with whiskers representing ±1 standard deviation. The black dot
 255 within the box represents the mean. Differences between SLB and non-SLB days were tested using
 256 a two-sample t-test. Statistical significances are denoted as *(*p* < 0.05), **(*p* < 0.01) and ***(*p* <
 257 0.001). For all panels except (h), the number adjacent to the significance symbol denotes the ratio
 258 of the mean value on SLB days to that on non-SLB days; in panel (h), it denotes the absolute
 259 difference between the means.



260

261 Figure 2. Relationship between HONO_{corr} and the important products of heterogeneous chemical
 262 processes during nocturnal SLB and non-SLB periods. HONO_{corr} denotes the corrected HONO
 263 concentration from secondary conversion. The products include (a, b) NO₃⁻ and (c, d) HCl. Blue and
 264 red dots represent observations during SLB days and non-SLB days, respectively. Each panel
 265 displays the linear regression fits and Pearson correlation coefficients (r) for the corresponding
 266 periods.

267

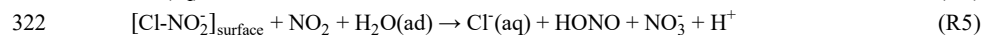
268 3.2 Enhanced rate of NO₂ uptake and its influencing factors

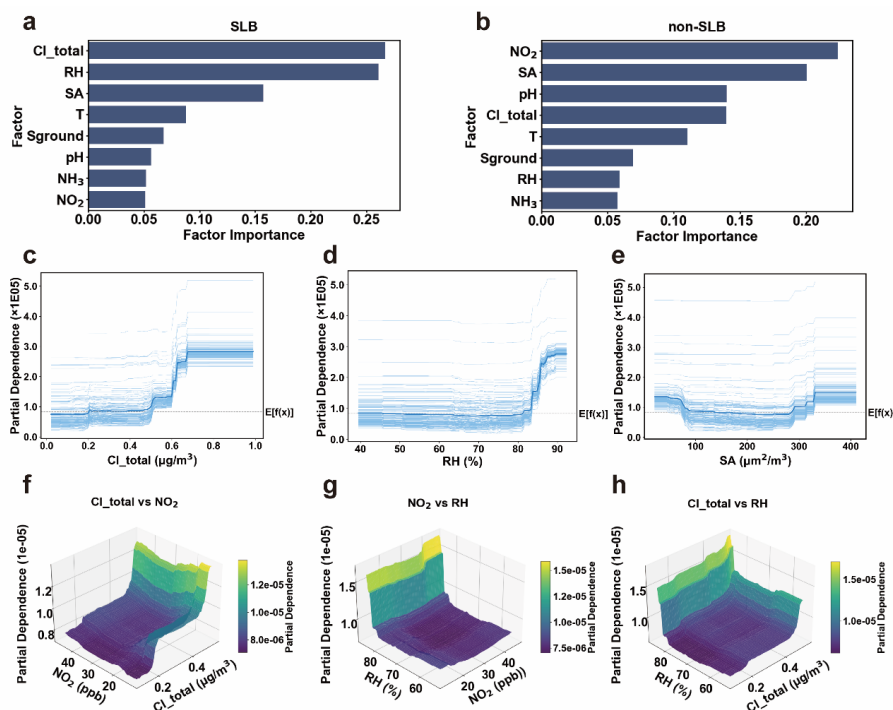
269 Using the variation of HONO_{corr}/NO₂ ratio, the values of kNO₂ on SLB days and non-SLB days
 270 were derived as Fig. S6. Overall, the average kNO₂ values on SLB days ($9.70 \times 10^{-6} \text{ s}^{-1}$) were
 271 significantly higher than those on non-SLB days ($6.72 \times 10^{-6} \text{ s}^{-1}$), by a factor of approximately 1.44.
 272 As presented in Table S4, a prolonged increase in the HONO_{corr}/NO₂ ratio was observed during 17
 273 of the 23 SLB days (see an example in Fig. S7). In contrast, this phenomenon was virtually absent
 274 on non-SLB days, indicating a sustained nocturnal enhancement of kNO₂ during SLB periods.
 275 Compared with existing field observations, the kNO₂ on SLB days was broadly consistent with the
 276 levels reported under the sea-case scenario in coastal cities of China such as Qingdao ($1.25 \times 10^{-5} \text{ s}^{-1}$)
 277 and Hong Kong ($8.81 \times 10^{-6} \text{ s}^{-1}$) (Yang et al., 2021; Zha et al., 2014), while it was markedly higher
 278 than those values observed in major non-coastal cities including Beijing ($7.78 \times 10^{-7} - 5.75 \times 10^{-6} \text{ s}^{-1}$)
 279 (Wang et al., 2017b; Zhang et al., 2020; Xuan et al., 2023; Jia et al., 2020; Zhang et al., 2022),
 280 Nanjing ($1.19 \times 10^{-6} - 2.22 \times 10^{-6} \text{ s}^{-1}$) (Zheng et al., 2020; Liu et al., 2019), and Guangzhou (4.44×10^{-6}
 281 $- 6.67 \times 10^{-6} \text{ s}^{-1}$) (Su et al., 2008; Li et al., 2012; Qin et al., 2009). The consistently higher kNO₂ in
 282 coastal areas implies that coastal atmospheric environments are likely more conducive to NO₂
 283 uptake.

284 A machine learning technique was used to further identify key drivers of the enhanced kNO₂
 285 on SLB days. Fig. S8 demonstrates that the constructed random forest model exhibits good



286 performance, successfully reproducing the calculated $k\text{NO}_2$ during both SLB and non-SLB periods,
287 making it suitable for subsequent factor analysis. The factor importance analyses (**Figs. 3a-3b**)
288 reveal that Cl_{total} (the sum of gaseous HCl and particulate Cl), RH, and SA were major drivers of
289 $k\text{NO}_2$ on SLB days, with Cl_{total} exhibiting the highest relative importance. Notably, the role of Cl_{total}
290 and RH diminished substantially on non-SLB days, underscoring the profound modulation of these
291 two influencing factors by the SLB circulation. **Fig 3c-3e** further elucidate the specific impacts of
292 these primary drivers on nocturnal $k\text{NO}_2$ under SLB conditions. Specifically, Cl_{total} exhibits a
293 positive correlation with $k\text{NO}_2$ (**Fig. 3c**). This phenomenon is likely attributable to the preferential
294 partitioning of chloride ions at the gas-aqueous interface of aerosols (Zhang et al., 2025a; Shen et
295 al., 2025; Wang et al., 2025a). The surface-bound Cl^- can attract gaseous NO_2 molecules (reaction
296 4) to form interfacial intermediates $[\text{Cl-NO}_2]_{\text{surface}}$, thereby facilitating the overall NO_2 uptake process.
297 Subsequent interaction analysis provides evidence that the mechanisms described in reactions 4-5,
298 originally identified under laboratory conditions, indeed occur within the coastal boundary layer.
299 **Fig. 3f** demonstrates that at a fixed NO_2 concentration, elevated chloride levels amplify the positive
300 effect of NO_2 molecules on $k\text{NO}_2$. This indicates that chloride ions actively promote the
301 heterogeneous uptake of NO_2 , consequently accelerating the $k\text{NO}_2$. Similar halogen-promoted
302 effect has also been revealed in NO_2 -initiated aqueous-phase oxidation of dissolved SO_2 at the air-
303 aqueous interface and of nitrate photolysis at the aqueous-phase surface (Wang et al., 2025a; Shen
304 et al., 2025). **Fig. 3d** shows a significant positive relationship exists between RH and $k\text{NO}_2$,
305 suggesting that moist sea breezes effectively supply the water molecules essential for the
306 heterogeneous NO_2 uptake. This finding aligns with previously reported field observations
307 highlighting RH-driven NO_2 uptake (Xuan et al., 2024). Analogous to Cl_{total} , the interaction between
308 RH and NO_2 reveals that at a constant NO_2 level, the positive impact of NO_2 on $k\text{NO}_2$ is enhanced
309 under elevated RH. It implies that RH also facilitates NO_2 uptake by promoting the interaction
310 between NO_2 molecules and heterogeneous interface. Furthermore, the interaction between Cl_{total}
311 and RH (**Fig. 3h**) reveals a positive synergistic effect, which partially explains the pronounced
312 increase in their relative importance for $k\text{NO}_2$ on SLB days. As a primary factor on both SLB and
313 non-SLB days, SA positively correlates with $k\text{NO}_2$ (**Fig. 3e**). This indicates that an increase in
314 aerosol surface area concentrations provides effective reaction interfaces for NO_2 uptake process,
315 consistent with most atmospheric heterogeneous processes (Wang et al., 2017a; Ma et al., 2026).
316 Moreover, **Fig. S9** show that on SLB days, concentrations of the major NO_2 uptake products (HONO
317 and NO_3^-) increased with those key factors including Cl_{total} , RH, and SA, providing additional
318 support for the above driving factor analysis. In general, the reasons underlying the enhanced $k\text{NO}_2$
319 on SLB days help to explain the multi-fold higher $k\text{NO}_2$ observed in coastal areas compared to non-
320 coastal urban areas, highlighting ambient chlorine levels and RH as non-negligible contributors.





323

324 Figure 3. Main and interaction effects of influencing factors for k_{NO_2} . Factor importance determined
 325 by the random forest (a) SLB days and (b) non-SLB days. Partial dependence plots for the primary
 326 drivers on SLB days: (c) Cl_{total} , (d) RH, and (e) SA. Interactions between key factors on SLB days:
 327 (f) Cl_{total} and NO_2 , (g) RH and Cl_{total} , and (h) RH and NO_2 . In panels (a-b), S_{ground} denotes ground
 328 surface areas calculated by $1/BLH$ (boundary layer height). In panels (c-h), partial dependence
 329 reflects the extent to which the influencing factors affect k_{NO_2} .

330

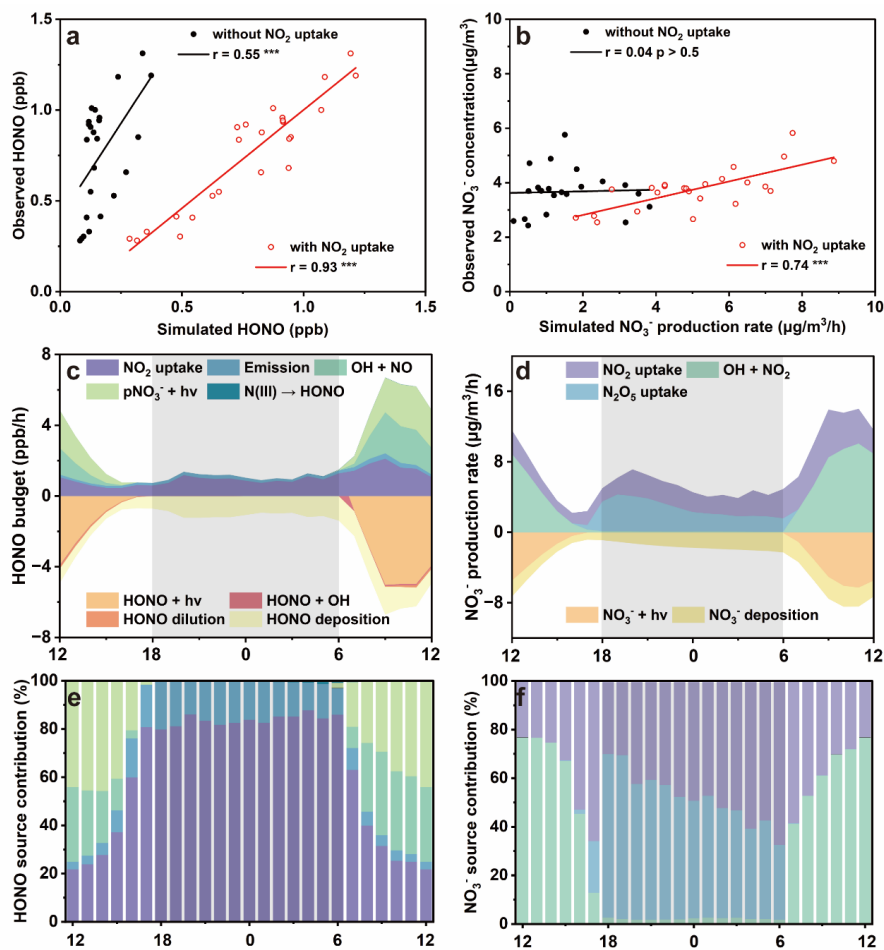
331 3.3 Enhanced NO_2 uptake promote the atmospheric reactive nitrogen cycle

332 The above correlations analysis suggests that NO_2 uptake could play an important role in the
 333 production of HONO and NO_3^- on SLB days. Since the HONO and NO_3^- formation were influenced
 334 by multiple meteorological factors and many atmospheric reaction pathways, a multiphase chemical
 335 box model was employed to evaluate the role of enhanced NO_2 uptake. As described in Methods,
 336 six simulation scenarios were set up. Incorporating NO_2 uptake mechanism, the model accurately
 337 reproduced HONO and NO_3^- observations on SLB days compared to without incorporating it (Figs.
 338 4a-4b), substantially improving r values from 0.55 to 0.93 and from statistically insignificant to
 339 0.74, respectively. Additionally, the NO_2 uptake could robustly explain the enhancements in both
 340 reactive atmospheric nitrogen species on SLB days across various k_{NO_2} quantiles (Fig. 10).
 341 Conversely, applying the current calculated k_{NO_2} to non-SLB days overpredicted HONO and NO_3^-
 342 levels (Fig. S11). This massive overestimation implies that the actual difference in k_{NO_2} between
 343 SLB and non-SLB days is likely greater than 1.44-fold, underscoring the amplified importance of
 344 NO_2 uptake on SLB days.

345 Figs.4c-4d illustrate the simulated HONO and NO_3^- budgets for the scenarios incorporating



346 NO₂ uptake on SLB days. Despite potential overestimations of non-SLB kNO₂, the mean NO₂
347 uptake rate remained significantly higher on SLB days than on non-SLB days, with an average rate
348 of 1.03 ppb/h (**Fig. S12**). During nighttime, NO₂ uptake accounted for 83.8% of HONO formation
349 (**Fig. 4e**). The predominance of NO₂ uptake in nocturnal HONO formation has also been observed
350 during PM pollution episodes in urban areas (Xuan et al., 2024; Jia et al., 2020). However, unlike
351 the chlorine-driven reason identified here, those prior cases were primarily attributed to favorable
352 heterogeneous reaction conditions, such as larger SA concentrations, lower BLH, and higher RH.
353 In addition to NO₂ uptake, primary emissions from vehicle exhaust, coal combustion, and biomass
354 burning are also recognized as major contributors to nighttime HONO in urban areas (Wang et al.,
355 2025b; Zhang et al., 2022). In this study, primary emissions contributed only 15.5% to nocturnal
356 HONO formation, substantially less than the contribution from NO₂ uptake. As for nighttime NO₃⁻
357 formation, many studies had indicated that N₂O₅ uptake was the dominant pathway in urban areas
358 (Chen et al., 2020; Wang et al., 2018). However, the situation changed under the impact of the
359 enhanced NO₂ uptake. **Fig. 4f** shows that NO₂ uptake contributed 47.9% to nocturnal NO₃⁻
360 formation, which was almost comparable to that of N₂O₅ uptake (50.0%). While chlorine can also
361 promote the uptake of N₂O₅ (Bertram and Thornton, 2009), the relative enhancement in the
362 contribution of NO₂ uptake to nocturnal NO₃⁻ formation was more pronounced. This might be
363 related to the suppression of N₂O₅ uptake caused by increased NO₃⁻ generating directly from NO₂
364 uptake. The increase in NO₃⁻ component of aerosol can shift the equilibrium between N₂O₅ and
365 NO₃⁻ toward N₂O₅, thereby reducing the contribution of N₂O₅ to NO₃⁻ formation (Bertram and
366 Thornton, 2009; Wagner et al., 2013). Additionally, the enhanced NO₂ uptake process also
367 competed for NO₂, an important precursor of N₂O₅ formation, especially in the NO₂-limited regime
368 for N₂O₅ formation (Lin et al., 2025), ultimately reducing the overall enhancement effect on N₂O₅
369 generation. Moreover, this comparable contribution of NO₂ and N₂O₅ uptake NO₃⁻ formation was
370 also found during fog events (Xu et al., 2024). Although the observed phenomenon was similar, the
371 dominant drivers differed between fog conditions and coastal SLB periods. The former was
372 primarily attributed to favorable uptake conditions such as abundant aerosol water content and high
373 surface area concentration, whereas the latter was more due to the enhancement effect of chlorine
374 levels and RH on the NO₂ uptake process. Overall, these results reveal the high contribution of NO₂
375 uptake to HONO and NO₃⁻ formation during SLB circulation periods, demonstrating that enhanced
376 NO₂ uptake can significantly influence the atmospheric reactive nitrogen cycle in coastal urban
377 areas.



378

379 Figure 4. Quantified results from the multiphase chemical box model. Relationship between (a)
 380 simulated HONO and observed HONO concentrations, (b) simulated NO_3^- production rate and
 381 observed NO_3^- concentration during SLB days, comparing the scenarios with and without
 382 considering heterogeneous NO_2 uptake mechanism. Diurnal variations of HONO (c) and NO_3^-
 383 budgets (d) during SLB days. Diurnal variations of source contributions to (e) HONO and (f) NO_3^- .
 384 The grey shaded areas represent the nighttime period.

385

386

4. Conclusions

387

388

389

390

391

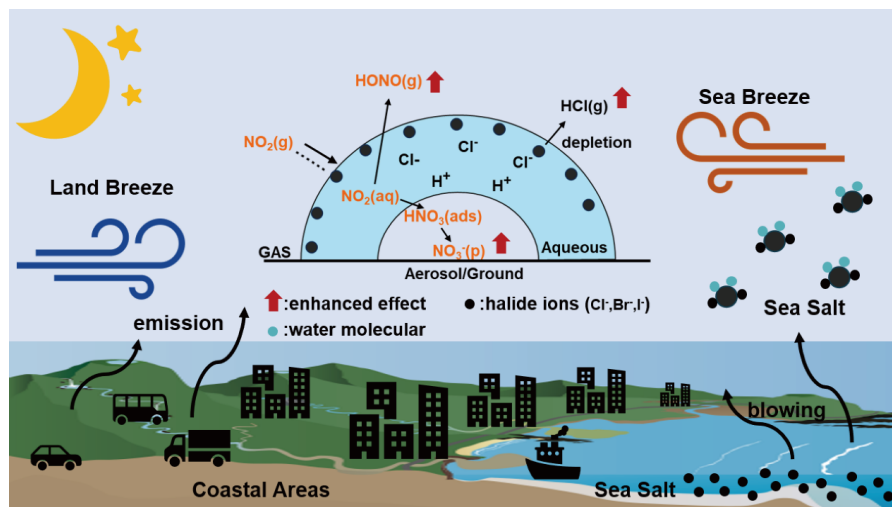
392

393

Overall, our observations show that nighttime sea-land breeze period in coastal urban areas were characterized by stronger sea-salt aerosol influence, higher relative humidity, and elevated HONO and nitrate concentrations. Nighttime conditions led to a significant enhancement in the NO_2 uptake rate constant, mainly driven by increased chlorine levels and relative humidity. Multiphase chemical box model simulations further confirmed that this enhanced NO_2 uptake promoted HONO and nitrate formation. Fig.5 illustrates a schematic diagram of chlorine-enhanced heterogeneous uptake of NO_2 during sea-land breeze days. Under the influence of strong sea-land breeze circulation, the



394 continuous influx of sea-salt aerosols transported by moist sea breezes leads to high chlorine levels
 395 during the night. Meanwhile, emission from vehicles and ships contribute substantial NO_2 , which
 396 accumulates in the coastal atmospheric boundary layer (Wen et al., 2023; Sun et al., 2025). Under
 397 these conditions, abundant chloride can effectively facilitate kNO_2 and promote the NO_2 uptake
 398 process, thereby influencing the formation of key atmospheric reactive nitrogen species, HONO and
 399 NO_3^- , as well as broader reactive nitrogen cycling. Notably, other sea-salt halides (Br, I) exhibit
 400 similar chemical properties to chlorine and may also contribute to the elevated kNO_2 (Zhang et al.,
 401 2025a). Additionally, our study focuses specifically on nocturnal NO_2 uptake to form HONO, given
 402 that daytime HONO formation involves more complex factors such as photo-enhanced
 403 heterogeneous reactions of NO_2 and nitrate photolysis (Stemmler et al., 2006; Han et al., 2016; Ye
 404 et al., 2017; Zhou et al., 2011), Future investigations are warranted to explicitly evaluate the impact
 405 of chlorine on daytime NO_2 uptake. Moreover, current air quality models often exhibit considerable
 406 biases in simulating secondary pollutants such as O_3 and $\text{PM}_{2.5}$ over coastal areas (Huang et al.,
 407 2025; Ma et al., 2025; Mao et al., 2022). One possible reason is that the influence of chlorine on
 408 chemical processes like NO_2 uptake has not yet been adequately considered. Given the dense traffic
 409 and substantial NO_2 emission in coastal cities of China, greater attention should be paid to the
 410 chlorine-enhanced NO_2 uptake process and its subsequent impact on nocturnal chemistry in coastal
 411 urban atmosphere.



412
 413 Figure 5. Schematic of the chlorine-enhanced heterogeneous uptake of NO_2 during sea-land breeze
 414 days in coastal areas. Red arrows, black solid circles, and blue solid circles represent the
 415 enhancement of the uptake process, halide ions and water molecular, respectively.

416
 417 **Code availability.** Data analysis methods are available on request from Jinsheng Chen
 418 (jschen@iue.ac.cn).

419
 420 **Data availability.** The dataset can be accessed at Zenodo website (Lin et al., 2026).

421
 422 **Author contributions:**



423 Z.L. contributed to the conceptualization, investigation, methodology, data curation, software,
424 analysis and writing of the original draft. L.X., and J.C. contributed to the data curation, reviewing
425 and editing the text, supervision, and funding acquisition X.Y., L.L., C.Y., X.J., Y.C., K.Z., F.Z.,
426 Z.C., G.C., X.F., and M.L. provided useful advice and revised the manuscript.

427 **Competing interests:**

428 The authors declare no competing interests.

429

430 **Acknowledgements.** The authors acknowledge all members of the atmospheric chemistry team at
431 the Institute of Urban Environment.

432

433 **Financial support.** This work was funded by the National Natural Science Foundation of China
434 (U22A20578), the guiding project of seizing the commanding heights of “self-purifying city” (IUE-
435 CERAE-202402), the National Key Research and Development Program (2022YFC3700304), STS
436 Plan Supporting Project of the Chinese Academy of Sciences in Fujian Province (2023T3013), and
437 Xiamen Atmospheric Environment Observation and Research Station of Fujian Province.

438

439 **References:**

440 Acker, K., Möller, D., Wieprecht, W., Meixner, F. X., Bohn, B., Gilge, S., Plass-Dülmer, C., and
441 Berresheim, H.: Strong daytime production of OH from HNO₂ at a rural mountain site, *Geophysical*
442 *Research Letters*. 33, <https://doi.org/10.1029/2005GL024643>, 2006.

443 Aliche, B., Geyer, A., Hofzumahaus, A., Holland, F., Konrad, S., Pätz, H. W., Schäfer, J., Stutz, J., Volz-
444 Thomas, A., and Platt, U.: OH formation by HONO photolysis during the BERLIOZ experiment, *Journal*
445 *of Geophysical Research: Atmospheres*. 108, PHO 3-1-PHO 3-17,
446 <https://doi.org/10.1029/2001JD000579>, 2003.

447 Bertram, T. H. and Thornton, J. A.: Toward a general parameterization of N₂O₅ reactivity on aqueous
448 particles: the competing effects of particle liquid water, nitrate and chloride, *Atmos. Chem. Phys.*, 9,
449 8351-8363, <https://doi.org/10.5194/acp-9-8351-2009>, 2009.

450 Breiman, L.: Random Forests, *Machine Learning*. 45, 5-32, <https://doi.org/10.1023/A:1010933404324>,
451 2001.

452 Cao, Y., Ma, Q., Chu, B., and He, H.: Homogeneous and heterogeneous photolysis of nitrate in the
453 atmosphere: state of the science, current research needs, and future prospects, *Frontiers of Environmental*
454 *Science & Engineering*. 17, 48, <https://doi.org/10.1007/s11783-023-1648-6>, 2022.

455 Carter, W. P. L., Atkinson, R., Winer, A. M., and Pitts Jr, J. N.: Experimental investigation of chamber-
456 dependent radical sources, *International Journal of Chemical Kinetics*. 14, 1071-1103, <https://doi.org/10.1002/kin.550141003>, 1982.

458 Chen, X., Wang, H., Lu, K., Li, C., Zhai, T., Tan, Z., Ma, X., Yang, X., Liu, Y., Chen, S., Dong, H., Li,
459 X., Wu, Z., Hu, M., Zeng, L., and Zhang, Y.: Field Determination of Nitrate Formation Pathway in Winter
460 Beijing, *Environmental Science & Technology*. 54, 9243-9253, <https://doi.org/10.1021/acs.est.0c00972>,
461 2020.

462 Chen, Y., Yang, C., Xu, L., Chen, J., Zhang, Y., Shi, J., Fan, X., Zheng, R., Hong, Y., and Li, M.: Chemical
463 composition of NR-PM₁ in a coastal city of Southeast China: Temporal variations and formation
464 pathways, *Atmospheric Environment*. 285, 119243, <https://doi.org/10.1016/j.atmosenv.2022.119243>,
465 2022.

466 Chen, Y., Yang, C., Xu, L., Fan, X., Shi, J., Zheng, R., Hong, Y., Li, M., Liu, T., Chen, G., Yin, L., and



- 467 Chen, J.: Variations of chemical composition of NR-PM1 under the influence of sea land breeze in a
468 coastal city of Southeast China, *Atmospheric Research*. 285, 106626, [https://doi.org/](https://doi.org/10.1016/j.atmosres.2023.106626)
469 [10.1016/j.atmosres.2023.106626](https://doi.org/10.1016/j.atmosres.2023.106626), 2023.
- 470 Cui, L., Li, R., Zhang, Y., Meng, Y., Fu, H., and Chen, J.: An observational study of nitrous acid (HONO)
471 in Shanghai, China: The aerosol impact on HONO formation during the haze episodes, *Science of The*
472 *Total Environment*. 630, 1057-1070, [https://doi.org/ 10.1016/j.scitotenv.2018.02.063](https://doi.org/10.1016/j.scitotenv.2018.02.063), 2018.
- 473 Gen, M., Zheng, H., Sun, Y., Xu, W., Ma, N., Su, H., Cheng, Y., Wang, S., Xing, J., Zhang, S., Xue, L.,
474 Xue, C., Mu, Y., Tian, X., Matsuki, A., and Song, S.: Rapid hydrolysis of NO₂ at High Ionic Strengths of
475 Deliquesced Aerosol Particles, *Environmental Science & Technology*. 58, 7904-7915,
476 <https://doi.org/10.1021/acs.est.3c08810>, 2024.
- 477 Goldstein, A., Kapelner, A., Bleich, J., and Pitkin, E.: Peeking Inside the Black Box: Visualizing
478 Statistical Learning With Plots of Individual Conditional Expectation, *Journal of Computational and*
479 *Graphical Statistics*. 24, 44-65, <https://doi.org/10.1080/10618600.2014.907095>, 2015.
- 480 Gregorutti, B., Michel, B., and Saint-Pierre, P.: Correlation and variable importance in random forests,
481 *Statistics and Computing*. 27, 659-678, <https://doi.org/10.1007/s11222-016-9646-1>, 2017.
- 482 Han, C., Yang, W., Wu, Q., Yang, H., and Xue, X.: Heterogeneous Photochemical Conversion of NO₂ to
483 HONO on the Humic Acid Surface under Simulated Sunlight, *Environmental Science & Technology*. 50,
484 5017-5023, <https://doi.org/10.1021/acs.est.5b05101>, 2016.
- 485 Hao, Q., Jiang, N., Zhang, R., Yang, L., and Li, S.: Characteristics, sources, and reactions of nitrous acid
486 during winter at an urban site in the Central Plains Economic Region in China, *Atmos. Chem. Phys.*, 20,
487 7087-7102, <https://doi.org/10.5194/acp-20-7087-2020>, 2020.
- 488 Hersbach, H., Bell, B., Berrisford, P., Hirahara, S., Horányi, A., Muñoz-Sabater, J., Nicolas, J., Peubey,
489 C., Radu, R., Schepers, D., Simmons, A., Soci, C., Abdalla, S., Abellan, X., Balsamo, G., Bechtold, P.,
490 Biavati, G., Bidlot, J., Bonavita, M., De Chiara, G., Dahlgren, P., Dee, D., Diamantakis, M., Dragani, R.,
491 Flemming, J., Forbes, R., Fuentes, M., Geer, A., Haimberger, L., Healy, S., Hogan, R. J., Hólm, E.,
492 Janisková, M., Keeley, S., Laloyaux, P., Lopez, P., Lupu, C., Radnoti, G., de Rosnay, P., Rozum, I.,
493 Vamborg, F., Villaume, S., and Thépaut, J.-N.: The ERA5 global reanalysis, *Quarterly Journal of the*
494 *Royal Meteorological Society*. 146, 1999-2049, [https://doi.org/ 10.1002/qj.3803](https://doi.org/10.1002/qj.3803), 2020.
- 495 Huang, L., Zhang, X., Emery, C., Mu, Q., Yarwood, G., Zhai, H., Sun, Z., Xue, S., Wang, Y., Fu, J. S.,
496 and Li, L.: Recommendations on benchmarks for numerical air quality model applications in China –
497 Part 2: Ozone and uncertainty analysis, *Atmos. Chem. Phys.*, 25, 4233-4249, [https://doi.org/10.5194/acp-](https://doi.org/10.5194/acp-25-4233-2025)
498 [25-4233-2025](https://doi.org/10.5194/acp-25-4233-2025), 2025.
- 499 Jia, C., Tong, S., Zhang, W., Zhang, X., Li, W., Wang, Z., Wang, L., Liu, Z., Hu, B., Zhao, P., and Ge,
500 M.: Pollution characteristics and potential sources of nitrous acid (HONO) in early autumn 2018 of
501 Beijing, *Science of The Total Environment*. 735, 139317, [https://doi.org/](https://doi.org/10.1016/j.scitotenv.2020.139317)
502 [10.1016/j.scitotenv.2020.139317](https://doi.org/10.1016/j.scitotenv.2020.139317), 2020.
- 503 Jungwirth, P. and Tobias, D. J.: Specific Ion Effects at the Air/Water Interface, *Chemical Reviews*. 106,
504 1259-1281, <https://doi.org/10.1021/cr0403741>, 2006.
- 505 Kleffmann, J., Kurtenbach, R., Lörzer, J., Wiesen, P., Kalthoff, N., Vogel, B., and Vogel, H.: Measured
506 and simulated vertical profiles of nitrous acid—Part I: Field measurements, *Atmospheric Environment*.
507 37, 2949-2955, [https://doi.org/10.1016/S1352-2310\(03\)00242-5](https://doi.org/10.1016/S1352-2310(03)00242-5), 2003.
- 508 Knipping, E. M., Lakin, M. J., Foster, K. L., Jungwirth, P., Tobias, D. J., Gerber, R. B., Dabdub, D., and
509 Finlayson-Pitts, B. J.: Experiments and Simulations of Ion-Enhanced Interfacial Chemistry on Aqueous
510 NaCl Aerosols, *Science*. 288, 301-306, <https://doi.org/10.1126/science.288.5464.301>, 2000.



- 511 Kulmala, M., Petäjä, T., Nieminen, T., Sipilä, M., Manninen, H. E., Lehtipalo, K., Dal Maso, M., Aalto,
512 P. P., Junninen, H., Paasonen, P., Riipinen, I., Lehtinen, K. E. J., Laaksonen, A., and Kerminen, V.-M.:
513 Measurement of the nucleation of atmospheric aerosol particles, *Nature Protocols*. 7, 1651-1667,
514 <https://doi.org/10.1038/nprot.2012.091>, 2012.
- 515 Lee, Y. N. and Schwartz, S. E.: Reaction kinetics of nitrogen dioxide with liquid water at low partial
516 pressure, *The Journal of Physical Chemistry*. 85, 840-848, <https://doi.org/10.1021/j150607a022>, 1981.
- 517 Li, L., Lin, Z., Li, M., Fan, X., Yang, C., Hou, A., Chen, Y., Xu, L., Hong, Y., and Chen, J.: Importance
518 of Methanesulfonic Acid in New Particle Formation in a Coastal City of Southeast China, *Geophysical
519 Research Letters*. 52, e2025GL117238, <https://doi.org/10.1029/2025GL117238>, 2025.
- 520 Li, X., Brauers, T., Häseler, R., Bohn, B., Fuchs, H., Hofzumahaus, A., Holland, F., Lou, S., Lu, K. D.,
521 Rohrer, F., Hu, M., Zeng, L. M., Zhang, Y. H., Garland, R. M., Su, H., Nowak, A., Wiedensohler, A.,
522 Takegawa, N., Shao, M., and Wahner, A.: Exploring the atmospheric chemistry of nitrous acid (HONO)
523 at a rural site in Southern China, *Atmos. Chem. Phys.*, 12, 1497-1513, [https://doi.org/10.5194/acp-12-
524 1497-2012](https://doi.org/10.5194/acp-12-1497-2012), 2012.
- 525 Lin, Z., Li, L., Xu, L., Ji, X., Zhang, K., Yang, C., Chen, G., Fan, X., and Chen, J.: Unexpected Daytime
526 N₂O₅ in Urban Areas: Formation Mechanisms and Environmental Impacts, *Geophysical Research
527 Letters*. 53, e2025GL121461, <https://doi.org/10.1029/2025GL121461>, 2026a.
- 528 Lin, Z., Ji, X., Xu, L., Chen, G., Yang, C., Zhang, K., Zhang, F., Li, L., Chen, Y., and Chen, J.: Enhanced
529 NO₂-driven multiphase formation of particulate nitrate and sulfate under high-humidity conditions, *npj
530 Climate and Atmospheric Science*. 9, 76, <https://doi.org/10.1038/s41612-026-01352-5>, 2026b.
- 531 Lin, Z., Ying, C., Xu, L., Ji, X., Zhang, K., Zhang, F., Chen, G., Li, L., Yang, C., Chen, Y., Chen, Z., and
532 Chen, J.: Measurement report: High contribution of N₂O₅ uptake to particulate nitrate formation in NO₂-
533 limited urban areas, *Atmos. Chem. Phys.*, 25, 17747-17759, <https://doi.org/10.5194/acp-25-17747-2025>,
534 2025.
- 535 Lin, Z., Xu, L., & Chen, J. (2026). Data for Chlorine enhances nocturnal heterogeneous uptake of NO₂
536 in coastal atmosphere under sea-land breeze circulation [Data set].
537 Zenodo. <https://doi.org/10.5281/zenodo.21037074>.
- 538 Liu, C., Wang, H., Li, L., Chen, X., Lu, X., and Fan, S.: Impacts of sea-land breeze on the coastal ozone
539 in the Pearl River Delta, China, *Journal of Environmental Sciences*.
540 <https://doi.org/10.1016/j.jes.2025.08.037>, 2025.
- 541 Liu, T. and Abbatt, J. P. D.: Oxidation of sulfur dioxide by nitrogen dioxide accelerated at the interface
542 of deliquesced aerosol particles, *Nature Chemistry*. 13, 1173-1177, [https://doi.org/10.1038/s41557-021-
543 00777-0](https://doi.org/10.1038/s41557-021-00777-0), 2021.
- 544 Liu, T., Hong, Y., Li, M., Xu, L., Chen, J., Bian, Y., Yang, C., Dan, Y., Zhang, Y., Xue, L., Zhao, M.,
545 Huang, Z., and Wang, H.: Atmospheric oxidation capacity and ozone pollution mechanism in a coastal
546 city of southeastern China: analysis of a typical photochemical episode by an observation-based model,
547 *Atmos. Chem. Phys.*, 22, 2173-2190, <https://doi.org/10.5194/acp-22-2173-2022>, 2022.
- 548 Liu, Y., Nie, W., Xu, Z., Wang, T., Wang, R., Li, Y., Wang, L., Chi, X., and Ding, A.: Semi-quantitative
549 understanding of source contribution to nitrous acid (HONO) based on 1 year of continuous observation
550 at the SORPES station in eastern China, *Atmos. Chem. Phys.*, 19, 13289-13308,
551 <https://doi.org/10.5194/acp-19-13289-2019>, 2019.
- 552 Ma, W., Chen, X., Wang, Y., Zhang, Y., Zheng, F., Li, J., Hua, C., Zhao, Z., Yuan, Q., Wu, J., Jiang, J.,
553 Ye, P., Kulmala, M., Worsnop, D. R., Yang, H., and Liu, Y.: High Aerosol Ionic Strength Possibly
554 Affecting Nocturnal Chlorine Formation via Heterogeneous Reaction in Urban Beijing, *Environmental*



- 555 Science & Technology. 60, 902-912, <https://doi.org/10.1021/acs.est.5c09187>, 2026.
- 556 Ma, X., Liu, H., and Peng, Z.: Improving PM_{2.5} and PM₁₀ predictions in China from WRF_Chem
557 through a deep learning method: Multiscale depth-separable UNet, Environmental Pollution. 364,
558 125344, <https://doi.org/10.1016/j.envpol.2024.125344>, 2025.
- 559 Mao, J., Li, L., Li, J., Sulaymon, I. D., Xiong, K., Wang, K., Zhu, J., Chen, G., Ye, F., Zhang, N., Qin, Y.,
560 Qin, M., and Hu, J.: Evaluation of Long-Term Modeling Fine Particulate Matter and Ozone in China
561 During 2013–2019, Frontiers in Environmental Science. Volume 10 - 2022,
562 <https://doi.org/10.3389/fenvs.2022.872249>, 2022.
- 563 Nie, W., Yan, C., Huang, D. D., Wang, Z., Liu, Y., Qiao, X., Guo, Y., Tian, L., Zheng, P., Xu, Z., Li, Y.,
564 Xu, Z., Qi, X., Sun, P., Wang, J., Zheng, F., Li, X., Yin, R., Dallenbach, K. R., Bianchi, F., Petäjä, T.,
565 Zhang, Y., Wang, M., Schervish, M., Wang, S., Qiao, L., Wang, Q., Zhou, M., Wang, H., Yu, C., Yao, D.,
566 Guo, H., Ye, P., Lee, S., Li, Y. J., Liu, Y., Chi, X., Kerminen, V.-M., Ehn, M., Donahue, N. M., Wang, T.,
567 Huang, C., Kulmala, M., Worsnop, D., Jiang, J., and Ding, A.: Secondary organic aerosol formed by
568 condensing anthropogenic vapours over China's megacities, Nature Geoscience. 15, 255-261,
569 <https://doi.org/10.1038/s41561-022-00922-5>, 2022.
- 570 Piatkowski, L., Zhang, Z., Backus, E. H. G., Bakker, H. J., and Bonn, M.: Extreme surface propensity of
571 halide ions in water, Nature Communications. 5, 4083, <https://doi.org/10.1038/ncomms5083>, 2014.
- 572 Qin, M., Xie, P., Su, H., Gu, J., Peng, F., Li, S., Zeng, L., Liu, J., Liu, W., and Zhang, Y.: An observational
573 study of the HONO–NO₂ coupling at an urban site in Guangzhou City, South China, Atmospheric
574 Environment. 43, 5731-5742, <https://doi.org/10.1016/j.atmosenv.2009.08.017>, 2009.
- 575 Qu, R. and Han, G.: A critical review of the variation in rainwater acidity in 24 Chinese cities during
576 1982–2018, Elementa: Science of the Anthropocene. 9, 00142,
577 <https://doi.org/10.1525/elementa.2021.00142>, 2021.
- 578 Seinfeld, J. H., Pandis, S. N., and Noone, K. J.: Atmospheric Chemistry and Physics: From Air Pollution
579 to Climate Change, Physics Today. 51, 88-90, 1998.
- 580 Shen, H., Li, Q., Xu, F., Xue, L., Hu, Y., Saiz-Lopez, A., Wang, W., and Wang, T.: Aerosol iodide
581 accelerates reactive nitrogen cycling in the marine atmosphere, Nature Communications. 16, 8148,
582 <https://doi.org/10.1038/s41467-025-63420-3>, 2025.
- 583 Shi, X., Ge, Y., Zheng, J., Ma, Y., Ren, X., and Zhang, Y.: Budget of nitrous acid and its impacts on
584 atmospheric oxidative capacity at an urban site in the central Yangtze River Delta region of China,
585 Atmospheric Environment. 238, 117725, <https://doi.org/10.1016/j.atmosenv.2020.117725>, 2020.
- 586 Stemmler, K., Ammann, M., Donders, C., Kleffmann, J., and George, C.: Photosensitized reduction of
587 nitrogen dioxide on humic acid as a source of nitrous acid, Nature. 440, 195-198,
588 <https://doi.org/10.1038/nature04603>, 2006.
- 589 Su, H., Cheng, Y. F., Cheng, P., Zhang, Y. H., Dong, S., Zeng, L. M., Wang, X., Slanina, J., Shao, M., and
590 Wiedensohler, A.: Observation of nighttime nitrous acid (HONO) formation at a non-urban site during
591 PRIDE-PRD2004 in China, Atmospheric Environment. 42, 6219-6232, <https://doi.org/10.1016/j.atmosenv.2008.04.006>, 2008.
- 593 Sun, L., Zhang, J., Ducruet, C., Itoh, H., and Liu, X.: The impact of shipping activities on air quality and
594 residents' health in China's port cities, Journal of Transport Geography. 123, 104099, <https://doi.org/10.1016/j.jtrangeo.2024.104099>, 2025.
- 596 Wagner, N. L., Riedel, T. P., Young, C. J., Bahreini, R., Brock, C. A., Dubé, W. P., Kim, S., Middlebrook,
597 A. M., Öztürk, F., Roberts, J. M., Russo, R., Sive, B., Swarthout, R., Thornton, J. A., VandenBoer, T. C.,
598 Zhou, Y., and Brown, S. S.: N₂O₅ uptake coefficients and nocturnal NO₂ removal rates determined from



- 599 ambient wintertime measurements, *Journal of Geophysical Research: Atmospheres*. 118, 9331-9350,
600 [https://doi.org/ 10.1002/jgrd.50653](https://doi.org/10.1002/jgrd.50653), 2013.
- 601 Wang, G., Zhang, S., Wu, C., Zhu, T., Xu, X., Ge, S., Sun, H., Sun, Z., Wang, J., Ji, Y., Gao, J., Ren, Y.,
602 Li, H., Zhang, F., Wang, Y., and Seinfeld, J. H.: Atmospheric sulfate aerosol formation enhanced by
603 interfacial anions, *PNAS Nexus*. 4, pgaf058, <https://doi.org/10.1093/pnasnexus/pgaf058>, 2025a.
- 604 Wang, H., Lu, K., Guo, S., Wu, Z., Shang, D., Tan, Z., Wang, Y., Le Breton, M., Lou, S., Tang, M., Wu,
605 Y., Zhu, W., Zheng, J., Zeng, L., Hallquist, M., Hu, M., and Zhang, Y.: Efficient N₂O₅ uptake and NO₃
606 oxidation in the outflow of urban Beijing, *Atmos. Chem. Phys.*, 18, 9705-9721,
607 <https://doi.org/10.5194/acp-18-9705-2018>, 2018.
- 608 Wang, H., Lu, K., Chen, X., Zhu, Q., Chen, Q., Guo, S., Jiang, M., Li, X., Shang, D., Tan, Z., Wu, Y.,
609 Wu, Z., Zou, Q., Zheng, Y., Zeng, L., Zhu, T., Hu, M., and Zhang, Y.: High N₂O₅ Concentrations
610 Observed in Urban Beijing: Implications of a Large Nitrate Formation Pathway, *Environmental Science
& Technology Letters*. 4, 416-420, <https://doi.org/10.1021/acs.estlett.7b00341>, 2017a.
- 612 Wang, J., Zhang, X., Guo, J., Wang, Z., and Zhang, M.: Observation of nitrous acid (HONO) in Beijing,
613 China: Seasonal variation, nocturnal formation and daytime budget, *Science of The Total Environment*.
614 587-588, 350-359, [https://doi.org/ 10.1016/j.scitotenv.2017.02.159](https://doi.org/10.1016/j.scitotenv.2017.02.159), 2017b.
- 615 Wang, Y., Liu, P., Zhang, C., Xue, C., Zhao, X., Fu, S., Wu, Z., Song, Y., Wang, Y., Liu, C., and Mu, Y.:
616 Evaluating the contribution of residential coal combustion to atmospheric nitrous acid (HONO) in winter,
617 *Environmental Pollution*. 378, 126488, [https://doi.org/ 10.1016/j.envpol.2025.126488](https://doi.org/10.1016/j.envpol.2025.126488), 2025b.
- 618 Wen, Y., Liu, M., Zhang, S., Wu, X., Wu, Y., and Hao, J.: Updating On-Road Vehicle Emissions for China:
619 Spatial Patterns, Temporal Trends, and Mitigation Drivers, *Environmental Science & Technology*. 57,
620 14299-14309, <https://doi.org/10.1021/acs.est.3c04909>, 2023.
- 621 Wentzell, J. J. B., Schiller, C. L., and Harris, G. W.: Measurements of HONO during BAQS-Met, *Atmos.*
622 *Chem. Phys.*, 10, 12285-12293, <https://doi.org/10.5194/acp-10-12285-2010>, 2010.
- 623 Wolfe, G. M., Marvin, M. R., Roberts, S. J., Travis, K. R., and Liao, J.: The Framework for 0-D
624 Atmospheric Modeling (F0AM) v3.1, *Geosci. Model Dev.*, 9, 3309-3319, <https://doi.org/10.5194/gmd-9-3309-2016>, 2016.
- 626 Xie, J., Sun, J., Li, Y., Chan, P. W., Li, L., Huang, C., Tang, L., Fan, S., Zheng, Y., and Fan, Z.: Sea-land
627 breezes in the Guangdong- Hong Kong- Macau Greater Bay Area coastal zone from 2013 to 2022,
628 *Atmospheric Research*. 296, 107044, <https://doi.org/10.1016/j.atmosres.2023.107044>, 2023.
- 629 Xu, W., Kuang, Y., Xu, W., Liu, L., Xu, H., Wang, X., Liu, Y., Cheng, H., Zhang, X., Zhai, M., Liu, C.,
630 Liang, L., Zhang, G., Luo, B., Tao, J., Liu, J., Zhao, H., Ren, S., Zhou, G., Liu, P., Xu, X., and Sun, Y.:
631 Efficient Nitrate Formation in Fog Events Implicates Fog Interstitial Aerosols as Significant Drivers of
632 Atmospheric Chemistry, *Environmental Science & Technology*. 58, 22298-22311,
633 <https://doi.org/10.1021/acs.est.4c09078>, 2024.
- 634 Xuan, H., Liu, C., Zhang, P., Chu, B., Liang, L., Ma, Q., and He, H.: A Review of Laboratory Studies on
635 the Heterogeneous Chemistry of NO₂: Mechanisms and Uptake Kinetics, *The Journal of Physical
636 Chemistry A*. 129, 815-835, <https://doi.org/10.1021/acs.jpca.4c07943>, 2025.
- 637 Xuan, H., Zhao, Y., Ma, Q., Chen, T., Liu, J., Wang, Y., Liu, C., Wang, Y., Liu, Y., Mu, Y., and He, H.:
638 Formation mechanisms and atmospheric implications of summertime nitrous acid (HONO) during clean,
639 ozone pollution and double high-level PM_{2.5} and O₃ pollution periods in Beijing, *Science of The Total
640 Environment*. 857, 159538, [https://doi.org/ 10.1016/j.scitotenv.2022.159538](https://doi.org/10.1016/j.scitotenv.2022.159538), 2023.
- 641 Xuan, H., Liu, J., Zhao, Y., Cao, Q., Chen, T., Wang, Y., Liu, Z., Sun, X., Li, H., Zhang, P., Chu, B., Ma,
642 Q., and He, H.: Relative humidity driven nocturnal HONO formation mechanism in autumn haze events



643 of Beijing, *npj Climate and Atmospheric Science*. 7, 193, <https://doi.org/10.1038/s41612-024-00745-8>,
644 2024.

645 Yang, C., Dong, H., Chen, Y., Wang, Y., Fan, X., Tham, Y. J., Chen, G., Xu, L., Lin, Z., Li, M., Hong, Y.,
646 and Chen, J.: Machine Learning Reveals the Parameters Affecting the Gaseous Sulfuric Acid Distribution
647 in a Coastal City: Model Construction and Interpretation, *Environmental Science & Technology Letters*.
648 10, 1045-1051, <https://doi.org/10.1021/acs.estlett.3c00170>, 2023.

649 Yang, C., Dong, H., Chen, Y., Xu, L., Chen, G., Fan, X., Wang, Y., Tham, Y. J., Lin, Z., Li, M., Hong, Y.,
650 and Chen, J.: New Insights on the Formation of Nucleation Mode Particles in a Coastal City Based on a
651 Machine Learning Approach, *Environmental Science & Technology*. 58, 1187-1198,
652 <https://doi.org/10.1021/acs.est.3c07042>, 2024.

653 Yang, J., Shen, H., Guo, M.-Z., Zhao, M., Jiang, Y., Chen, T., Liu, Y., Li, H., Zhu, Y., Meng, H., Wang,
654 W., and Xue, L.: Strong marine-derived nitrous acid (HONO) production observed in the coastal
655 atmosphere of northern China, *Atmospheric Environment*. 244, 117948, <https://doi.org/10.1016/j.atmosenv.2020.117948>, 2021.

657 Ye, C., Zhang, N., Gao, H., and Zhou, X.: Photolysis of Particulate Nitrate as a Source of HONO and
658 NO_x, *Environmental Science & Technology*. 51, 6849-6856, <https://doi.org/10.1021/acs.est.7b00387>,
659 2017.

660 Zha, Q., Xue, L., Wang, T., Xu, Z., Yeung, C., Louie, P. K. K., and Luk, C. W. Y.: Large conversion rates
661 of NO₂ to HNO₂ observed in air masses from the South China Sea: Evidence of strong production at sea
662 surface?, *Geophysical Research Letters*. 41, 7710-7715, <https://doi.org/10.1002/2014GL061429>, 2014.

663 Zhang, R., Minamikawa, R., Gen, M., Singh, N., Daniel, D., Li, Y. J., Wang, X., and Chan, C. K.:
664 Evidence on Interfacial Reaction Governing NO₂ Hydrolysis in Deliquesced Aerosol Particles,
665 *Environmental Science & Technology*. 59, 11708-11719, <https://doi.org/10.1021/acs.est.5c05223>, 2025a.

666 Zhang, W., Tong, S., Jia, C., Wang, L., Liu, B., Tang, G., Ji, D., Hu, B., Liu, Z., Li, W., Wang, Z., Liu, Y.,
667 Wang, Y., and Ge, M.: Different HONO Sources for Three Layers at the Urban Area of Beijing,
668 *Environmental Science & Technology*. 54, 12870-12880, <https://doi.org/10.1021/acs.est.0c02146>, 2020.

669 Zhang, X., Tong, S., Jia, C., Zhang, W., Wang, Z., Tang, G., Hu, B., Liu, Z., Wang, L., Zhao, P., Pan, Y.,
670 and Ge, M.: Elucidating HONO formation mechanism and its essential contribution to OH during haze
671 events, *npj Climate and Atmospheric Science*. 6, 55, <https://doi.org/10.1038/s41612-023-00371-w>, 2023.

672 Zhang, X., Tong, S., Jia, C., Zhang, W., Li, J., Wang, W., Sun, Y., Wang, X., Wang, L., Ji, D., Wang, L.,
673 Zhao, P., Tang, G., Xin, J., Li, A., and Ge, M.: The Levels and Sources of Nitrous Acid (HONO) in Winter
674 of Beijing and Sanmenxia, *Journal of Geophysical Research: Atmospheres*. 127, e2021JD036278,
675 <https://doi.org/10.1029/2021JD036278>, 2022.

676 Zhang, Y., Zheng, F., Feng, Z., Lian, C., Wang, W., Fan, X., Ma, W., Lin, Z., Li, C., Zhang, G., Yan, C.,
677 Zhang, Y., Kerminen, V. M., Bianchi, F., Petäjä, T., Kangasluoma, J., Kulmala, M., and Liu, Y.:
678 Concentration and source changes of nitrous acid (HONO) during the COVID-19 lockdown in Beijing,
679 *Atmos. Chem. Phys.*, 24, 8569-8587, <https://doi.org/10.5194/acp-24-8569-2024>, 2024.

680 Zhang, Y., Liu, Y., Ma, W., Hua, C., Zheng, F., Lian, C., Wang, W., Xia, M., Zhao, Z., Li, J., Xie, J., Wang,
681 Z., Wang, Y., Chen, X., Zhang, Y., Feng, Z., Yan, C., Chu, B., Du, W., Kerminen, V.-M., Bianchi, F.,
682 Petäjä, T., Worsnop, D., and Kulmala, M.: Changing aerosol chemistry is redefining HONO sources,
683 *Nature Communications*. 16, 5238, <https://doi.org/10.1038/s41467-025-60614-7>, 2025b.

684 Zheng, J., Shi, X., Ma, Y., Ren, X., Jabbour, H., Diao, Y., Wang, W., Ge, Y., Zhang, Y., and Zhu, W.:
685 Contribution of nitrous acid to the atmospheric oxidation capacity in an industrial zone in the Yangtze
686 River Delta region of China, *Atmos. Chem. Phys.*, 20, 5457-5475, <https://doi.org/10.5194/acp-20-5457->



687 [2020](#), 2020.

688 Zhou, X., Zhang, N., TerAvest, M., Tang, D., Hou, J., Bertman, S., Alaghmand, M., Shepson, P. B.,

689 Carroll, M. A., Griffith, S., Dusanter, S., and Stevens, P. S.: Nitric acid photolysis on forest canopy surface

690 as a source for tropospheric nitrous acid, *Nature Geoscience*. 4, 440-443,

691 <https://doi.org/10.1038/ngeo1164>, 2011.

692